PERGAMON

International Journal of Multiphase Flow 27 (2001) 1247–1258

International Journal of Multiphase Flow

www.elsevier.com/locate/ijmulflow

Drag and lift forces acting on a spherical bubble in a linear shear flow ☆

R. Kurose [1], R. Misumi, S. Komori *

Department of Mechanical Engineering, Kyoto University, Kyoto 606-8501, Japan

Received 18 January 2000; received in revised form 7 December 2000

Abstract

The effects of fluid shear on drag and lift forces acting on a spherical bubble are studied for high particle Reynolds numbers of $0.5 \leqslant Re_p \leqslant 200$ by means of a three-dimensional numerical simulation, and the effects are compared with those for a solid particle. The results show that the fluid shear increases the drag acting on a bubble. On the other hand, the lift always acts from the lower fluid-velocity side to the higher fluid-velocity side, and tends to approach a constant value for high particle Reynolds numbers. Further, the asymptotic value of the lift increases with increasing fluid shear rate. Although the trend of the drag on a bubble against the fluid shear is similar to that on a solid particle, the trend of the lift is quite different. For a solid particle the direction of the lift changes from the higher fluid-velocity side to the lower fluid-velocity side with the increasing particle Reynolds number. The difference in the lift between a bubble and a solid particle can well be explained by taking account of pressure and viscous contributions to the lift.

Keywords: Lift; Shear flow; Bubble; Solid particle; Numerical simulation

1. Introduction

Since the dispersion phenomena of solid particles or bubbles are often seen in environmental and industrial shear flows, it is of importance to investigate the effects of mean shear on fluid

☆ This is an extended version of a paper that was first presented at ICMF'98 (Lyon, France) and subsequently selected by its Scientific Committee.

* Corresponding author. Tel.: +81-75-753-5244; fax: +81-75-753-5244.

E-mail address: komori@mech.kyoto-u.ac.jp (S. Komori).

[1] Present address: Yokosuka Research Laboratory, Central Research Institute of Electric Power Industry (CRIEPI), Kanagawa 240-0196, Japan.

0301-9322/01/$ - see front matter
PII: S0301-9322(00)00073-2

forces acting on a solid particle or a bubble in settling environmental problems and in designing industrial equipments.

When a solid particle or a bubble is moving in a shear flow, a transverse force referred to as lift is exerted. The lift acting on a spherical solid particle in a linear shear flow has often been investigated. Saffman (1965) derived an analytical expression of the lift by using a matched asymptotic expansion method under the assumptions of

$$\begin{aligned} &Re_{\mathrm{p}}\left(=\frac{2aU_{\mathrm{c}}}{\nu}\right)\ll 1, \quad Re_{\Omega}\left(=\frac{\Omega(2a)^2}{\nu}\right)\ll 1, \\ &Re_{\alpha}\left(=\frac{\alpha(2a)^2}{\nu}\right)\ll 1, \quad \varepsilon\left[=\frac{Re_{\alpha}^{1/2}}{Re_{\mathrm{p}}}=1.414\left(\frac{\alpha^*}{Re_{\mathrm{p}}}\right)^{1/2}\right]\gg 1 \end{aligned} \tag{1}$$

and McLaughlin (1991) extended Saffman's analysis to smaller ε. Here, a is the radius of the sphere, U_{c} is the fluid velocity on the streamline through the center of a sphere, ν is the kinematic viscosity, α is the fluid shear rate of the mean flow, Ω is the rotational angular speed of a sphere and α^* is the dimensionless shear rate of fluid defined by

$$\alpha^*=\left(\frac{a}{U_{\mathrm{c}}}\right)\left(\frac{\partial U}{\partial y}\right). \tag{2}$$

Dandy and Dwyer (1990) evaluated the lift for high particle Reynolds numbers of $0.1\leqslant Re_{\mathrm{p}}\leqslant 100$ by means of a three-dimensional numerical simulation of a linear shear flow around a spherical solid particle, and Mei (1992) proposed an approximate expression for the lift on the basis of the results of Saffman (1965) and Dandy and Dwyer (1990). Recently, Komori and Kurose (1996) and Kurose and Komori (1999) also tackled the same problem by using a three-dimensional numerical simulation for higher particle Reynolds numbers of $0.5\leqslant Re_{\mathrm{p}}\leqslant 500$, and found an interesting behavior of lift; the direction of lift changes from the higher fluid-velocity side to the lower fluid-velocity side with increasing Re_{p}.

On the other hand, the studies on the shear lift acting on a bubble for high particle Reynolds numbers are extremely limited. Mei and Klausner (1994) obtained an expression of the lift on a spherical bubble in a linear shear flow by combining the results for a solid particle in a viscous flow by McLaughlin (1991) and Mei (1992) with the results for a bubble in an inviscid flow by Auton (1987). Recently, Ligendre and Magnaudet (1998) estimated the lift by using a three-dimensional numerical simulation. According to their results, the lift always acts to the higher fluid-velocity side independent of the particle Reynolds number, and the behavior of the lift on a bubble is quite different from that on a solid particle. However, the reason why the lift generation mechanism is different between a bubble and a solid particle has not been clarified.

The purpose of this study is, therefore, to investigate the effects of fluid shear on the lift acting on a spherical bubble in a viscous linear shear flow for high particle Reynolds numbers by means of a three-dimensional numerical simulation, and to clarify the difference in the lift generation mechanism between a bubble and a solid particle. The computations for a bubble were carried out for $0.5\leqslant Re_{\mathrm{p}}\leqslant 200$, and the results are compared with those of Kurose and Komori (1999) for a solid particle. In addition, the variations of the drag acting on a bubble against the particle Reynolds number and fluid shear rate were investigated.

2. Numerical simulation

The flow geometry and coordinate system for the present computations are shown in Fig. 1. The imposed flow is a linear shear flow around a spherical bubble. The bubble is assumed to be so small that the deformation can be neglected. The three-dimensional unsteady Navier–Stokes (NS) equations in cylindrical coordinates are given by

$$\begin{aligned}
&\frac{\partial U}{\partial t}+(\mathbf{V}\cdot\nabla)U=-\frac{\partial p}{\partial x}+\frac{2}{Re_{\mathrm{p}}}\nabla^2 U,\\
&\frac{\partial V}{\partial t}+(\mathbf{V}\cdot\nabla)V-\frac{V^2}{r}=-\frac{\partial p}{\partial r}+\frac{2}{Re_{\mathrm{p}}}\left(\nabla^2 V-\frac{V}{r^2}-\frac{2}{r^2}\frac{\partial V}{\partial\theta}\right),\\
&\frac{\partial W}{\partial t}+(\mathbf{V}\cdot\nabla)W+\frac{VW}{r}=-\frac{1}{r}\frac{\partial p}{\partial\theta}+\frac{2}{\mathrm{Re}_{\mathrm{p}}}\left(\nabla^2 W-\frac{W}{r^2}+\frac{2}{r^2}\frac{\partial W}{\partial\theta}\right).
\end{aligned}\tag{3}$$

The NS equations were directly solved using a finite difference scheme based on the marker and cell (MAC) method. By taking divergence of the NS equations, the dimensionless pressure-Poisson (PP) equation was derived as follows:

$$\nabla^2 p=\frac{\partial D}{\partial t}-\nabla\cdot[(\mathbf{V}\cdot\nabla)\mathbf{V}]+\frac{2}{Re_{\mathrm{p}}}\nabla^2 D.\tag{4}$$

The NS equations and the PP equation were solved alternately. Here D, $\mathbf{V}$ and ∇^2 are defined by

$$\begin{aligned}
&D=\nabla\cdot\mathbf{V},\\
&\mathbf{V}=(V_x,V_r,V_\theta)=(U,V,W),\\
&\nabla^2=\frac{\partial^2}{\partial x}+\frac{1}{r}\frac{\partial}{\partial r}\left(r\frac{\partial}{\partial r}\right)+\frac{1}{r^2}\frac{\partial^2}{\partial\theta^2}.
\end{aligned}\tag{5}$$

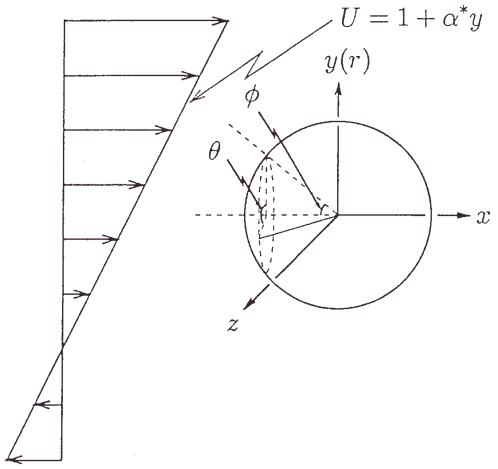

Fig. 1. Coordinate system for a spherical bubble in a linear shear flow.

The numerical procedure used here was essentially the same as that used in Hanazaki (1988) and Kurose and Komori (1999). The boundary condition on the bubble surface is given by a slip condition

$$\mathbf{V}\cdot\mathbf{n}=0,\quad \mathbf{n}\times(\boldsymbol{\tau}\cdot\mathbf{n})=0\quad \text{for } r=a, \tag{6}$$

whereas a no-slip condition ($\mathbf{V}=0$ for $r=a$) is used for a solid particle. Here $\mathbf{n}$ is the outward unit normal to the bubble surface, and $\boldsymbol{\tau}$ is the viscous stress tensor. The boundary condition of velocity upstream of a bubble was given in a dimensionless form by

$$U=1+\alpha^{*}y \tag{7}$$

and the velocity condition on the outer boundary, except upstream, is

$$\frac{\partial\mathbf{V}}{\partial x}=0. \tag{8}$$

By using a grid generation method developed by Thames et al. (1977), grid points were concentrated near the bubble surface in the (x,r)-plane. The maximum sizes of the computational domain were 20 and 10 radii in the x and r directions, respectively. The (x,r,θ)-coordinate system was transformed to the (η,ζ,θ)-coordinate system with an equal grid spacing (Fig. 2). The grid points used in this study were $35\times61\times48$ in the η, ζ and θ $(0\leqslant\theta\leqslant2\pi)$ directions. To accurately simulate the flow around a bubble, several mesh points at least are required in the boundary layer. By using the above grid generation method, ten or more than ten mesh points existed in the depth of the boundary layer which can be estimated by $1/Re_{\mathrm{p}}^{1/2}$. The transformed governing equations were discretized to construct the finite difference formulation. The nonlinear terms in the NS equations were approximated by a third-order scheme of Kawamura and Kuwahara (1984), and the other spatial derivatives were approximated by a second-order central difference scheme. The dimensionless time step Δt was 0.01.

The drag and lift, F_{D} and F_{L}, are the components of the fluid force acting on the spherical bubble in the x and y directions, and they can be calculated by the sum of the pressure and viscous force contributions

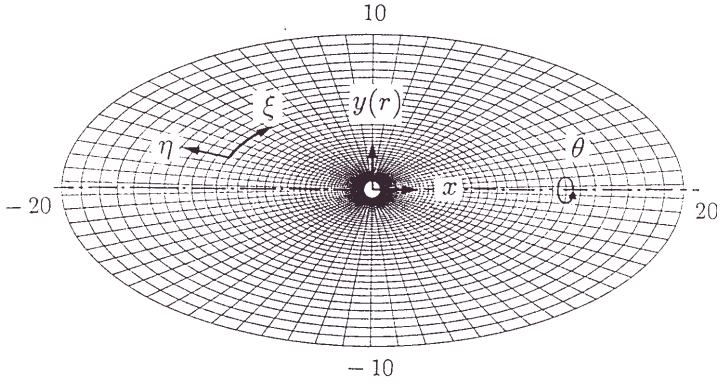

Fig. 2. Side view of numerical grids on the center plane ($z=0$).

$$F_i = F_{i,\mathrm{p}} + F_{i,\mathrm{f}} = -\int_S p\mathbf{e}_i \cdot \mathbf{n}\,\mathrm{d}S + \int_S \mathbf{n}\cdot\boldsymbol{\tau}\cdot\mathbf{e}_i\,\mathrm{d}S. \tag{9}$$

The tangential stress $\mathbf{n}\times(\boldsymbol{\tau}\cdot\mathbf{n})$ is zero on the bubble surface (see Eq. (1)), and the viscous force consists of normal stress $\mathbf{n}\cdot\boldsymbol{\tau}\cdot\mathbf{n}$. The drag and lift coefficients, C_D and C_L, are defined by

$$C_i = \frac{F_i}{(1/2)\rho_\mathrm{f} U_\mathrm{c}^2 \pi a^2}, \tag{10}$$

where ρ_f is the fluid density.

The computations were performed for particle Reynolds numbers of $Re_\mathrm{p} = 0.5$, $1, 2, 5, 10, 20, 50, 100$ and 200 and for fluid shear rates of $\alpha^* = 0, 0.1, 0.2$ and 0.4. The CPU time required to establish a quasi-steady state for each case was about 2000 s on an NEC SX-3 supercomputer of the Center for the Global Environmental Research, National Institute for Environmental Studies.

3. Results and discussion

3.1. Drag

Fig. 3 shows the variation of the drag coefficient C_D for a bubble in a uniform unsheared flow against the particle Reynolds number Re_p, together with that for a solid particle predicted by Kurose and Komori (1999). The analytical solutions by Stoke's assumption ($Re_\mathrm{p} \ll 1$) are given by

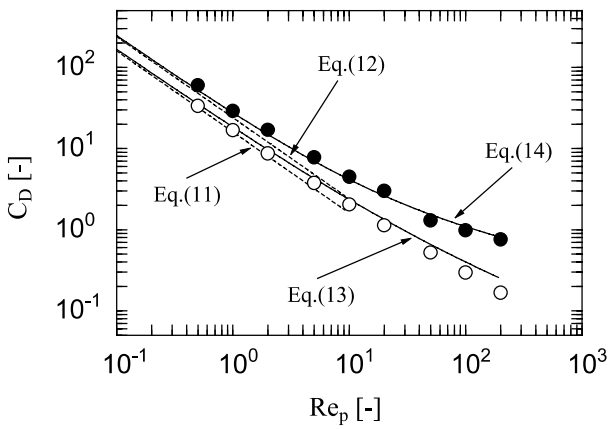

Fig. 3. Comparison of drag coefficient C_D in a uniform unsheared flow for a bubble with that for a solid particle: (○) bubble; (●) solid particle. The solid and dashed lines show the predictions by using the empirical expressions of Moore (1963) and Clift et al. (1987), and the analytical expressions based on Stoke's assumption, respectively.

$$C_{\mathrm{D,Bubble}} = \frac{16}{\mathrm{Re_p}}, \tag{11}$$

$$C_{\mathrm{D,Particle}} = \frac{24}{Re_{\mathrm{p}}}, \tag{12}$$

and the empirical predictions by Moore (1963) and Clift et al. (1987) (Magnaudet et al., 1995) are written by

$$C_{\mathrm{D,Bubble}} = \frac{16}{Re_{\mathrm{p}}}\left(1 + 0.15Re_{\mathrm{p}}^{0.5}\right), \tag{13}$$

$$C_{\mathrm{D,Particle}} = \frac{24}{Re_{\mathrm{p}}}\left(1 + 0.15Re_{\mathrm{p}}^{0.687}\right). \tag{14}$$

The analytical solutions and empirical predictions are also shown in the same figure. The present C_{D} for a bubble, as well as C_{D} for a solid particle (Kurose and Komori, 1999), generally agrees with the empirical predictions although for a bubble the difference between numerical and empirical results becomes larger at high particle Reynolds numbers of $Re_{\mathrm{p}} > 50$.

Fig. 4 shows the effect of fluid shear rate α^* on the drag coefficient C_{D} for a bubble in a linear shear flow. At a fixed value of Re_{p}, C_{D} increases with increasing α^*, and the dependency of C_{D} on α^* is more obvious for higher Re_{p}. This is clearly seen in the distribution of C_{D} against α^* for $Re_{\mathrm{p}} = 200$ (Fig. 5). The trend of C_{D} with α^* is similar to that for a solid particle given in Kurose and Komori (1999).

3.2. Lift

Fig. 6 compares the lift coefficient C_{L} for a bubble in a linear shear flow with C_{L} for a solid particle from Kurose and Komori (1999). The results obtained by Ligendre and Magnaudet (1998) and Mei and Klausner (1994) for a bubble and by McLaughlin (1991) for a solid particle are also shown in the figure. The expressions of Mei and Klausner (1994) and McLaughlin (1991) are given by

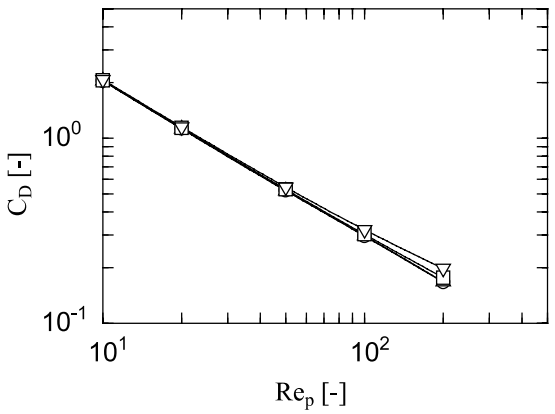

Fig. 4. Drag coefficient C_{D} for a bubble in a linear shear flow: (○) $\alpha^* = 0$; (△) $\alpha^* = 0.1$; (□) $\alpha^* = 0.2$; (▽) $\alpha^* = 0.4$.

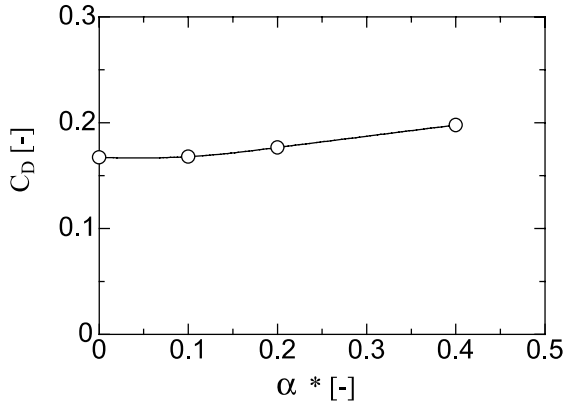

Fig. 5. Effect of fluid shear rate α^* on drag coefficient C_D for a bubble at $Re_p = 200$.

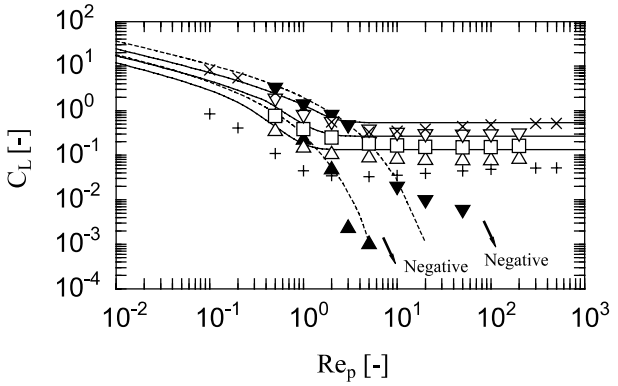

Fig. 6. Comparison of lift coefficient C_L in a linear shear flow for a bubble (open symbols) with that for a solid particle (closed symbols): (△, ▲) $\alpha^* = 0.1$; (□) $\alpha^* = 0.2$; (▽, ▼) $\alpha^* = 0.4$. The symbols (+) and (×) show the predictions for $\alpha^* = 0.04$ and 0.4 by Ligendre and Magnaudet (1998). The solid and dashedlines show the predictions for $\alpha^* = 0.1, 0.2$ and 0.4 by Mei and Klausner (1994), and for $\alpha^* = 0.1$ and 0.4 by McLaughlin (1991), respectively.

$$C_{L,M\text{-}K} = \alpha^{*1/2}\left\{\left[\frac{1.72J(\varepsilon)\sqrt{2\alpha^*/Re_p}}{Re_p^{1/2}}\right]^2 + \left(\frac{4}{3}\alpha^{*1/2}\right)^2\right\}^{1/2}, \tag{15}$$

$$C_{L,Mc} = 0.443J(\varepsilon)\cdot C_{L,Sa}, \tag{16}$$

where the subscripts M–K, Mc and Sa denote the results of Mei and Klausner (1994), McLaughlin (1991) and Saffman (1965), respectively. $C_{L,Sa}$ in (16) is given by

$$C_{L,Sa} = 5.816\left(\frac{|\alpha^*|}{Re_p}\right)^{1/2} \tag{17}$$

and $J(\varepsilon)$ is the empirical expression obtained by using a table of $J(\varepsilon)$ vs. ϵ in McLaughlin (1991)

$$J(\varepsilon) = 0.6765\{1 + \tanh[2.5\log_{10}(\varepsilon + 0.191)]\}\{0.667 + \tanh[6(\varepsilon - 0.32)]\}. \tag{18}$$

To derive (15), the analysis of a viscous linear shear flow around a solid particle by McLaughlin (1991) was generalized to be applicable to a bubble for low particle Reynolds numbers, and the analysis of a bubble in an inviscid linear shear flow by Auton (1987) was used for high particle Reynolds numbers. In the analysis of Auton (1987), the lift on a bubble is assumed to be linear against α^* in the large limit of Re_p.

As shown in Fig. 6, the lift on a bubble is always positive and acts to the higher fluid-velocity side. The C_L decreases with increasing Re_p ($Re_p \leqslant 5$), and it tends to approach a constant value for larger particle Reynolds numbers. It is also found from the variation of C_L against α^* for $Re_p = 200$ in Fig. 7 that the asymptotic value linearly increases with α^*. The trends of C_L with Re_p and α^* are very similar to those by Ligendre and Magnaudet (1998) and Mei and Klausner (1994). Ligendre and Magnaudet (1998) suggested that as Re_p increases, C_L^* [$= (3C_L)/(8\alpha^*)$] approaches Auton (1987)'s solution of $C_L^* = 0.5$, which was derived for a spherical bubble in an inviscid linear shear flow with $\alpha^* \to 0$. However, the results were not confirmed in the present study. The present C_L^* at $Re_p = 200$ was about 0.3 independent of α^* and less than 0.5 of Ligendre and Magnaudet (1998), although C_L^* may approach the value of 0.5 for much higher Re_p.

Komori and Kurose (1996) and Kurose and Komori (1999) found that C_L for a spherical solid particle in a linear shear flow becomes negative for high particle Reynolds numbers, and explained the negative C_L by investigating pressure and viscous contributions, $C_{L,p}$ and $C_{L,f}$, to the total lift C_L. The results suggest that the difference in the lift generation mechanism between a bubble and a solid particle may be caused by the effects of pressure and viscous force. Therefore, the variations of $C_{L,p}$, $C_{L,f}$ and C_L with Re_p for a bubble together with those for a solid particle are shown in Fig. 8 for $\alpha^* = 0.4$. For a solid particle, C_L changes its sign from positive to negative with increasing Re_p, since both of $C_{L,p}$ and $C_{L,f}$ become negative in the range $1 \leqslant Re_p \leqslant 100$. On the other hand, C_L for a bubble is positive independent of Re_p because $C_{L,p}$ consistently keeps a positive constant value although $C_{L,f}$ rapidly decreases to zero with increasing Re_p. Furthermore, it is found that for a bubble with high particle Reynolds number, $C_{L,p}$ is more dominant than $C_{L,f}$.

Fig. 9 shows the surface contours of the component for the pressure and viscous force in the y direction per unit area of the surface; pressure lift defined by $-p\mathbf{e}_y \cdot \mathbf{n}$ and viscous lift by $\boldsymbol{\tau} \cdot \mathbf{n} \cdot \mathbf{e}_y$, for $\alpha^* = 0.2$ on a bubble at $Re_p = 200$ and on a solid particle at $Re_p = 1$ and 200. The red and blue

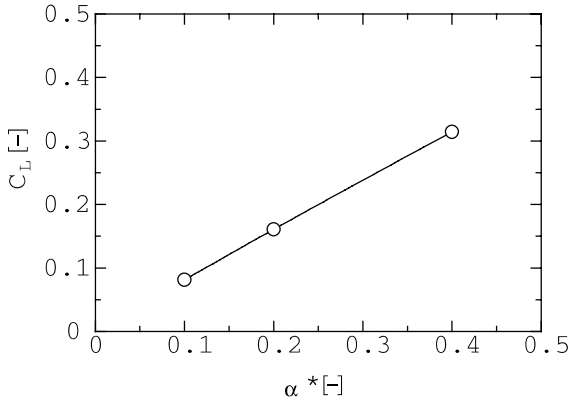

Fig. 7. Effect of fluid shear rate α^* on lift coefficient C_L for a bubble at $Re_p = 200$.

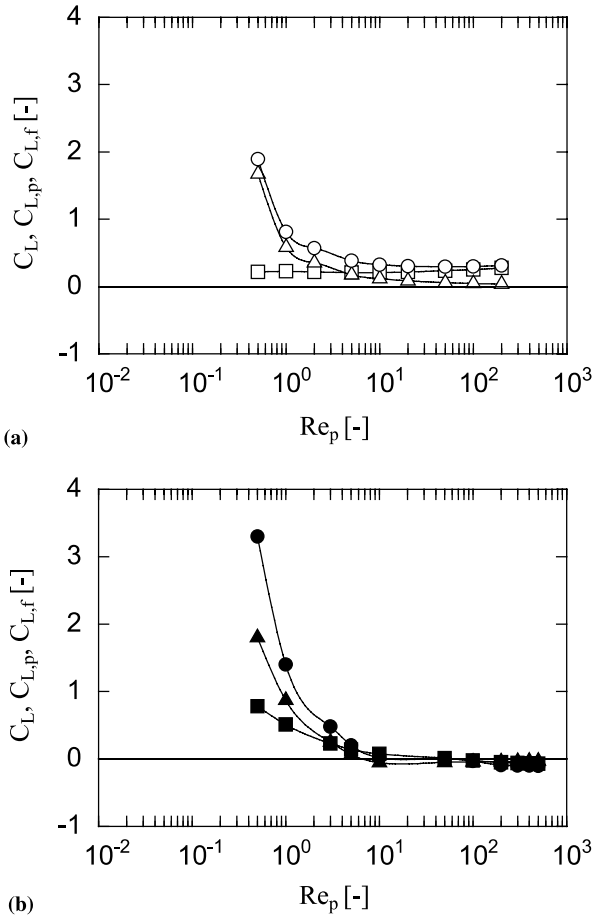

Fig. 8. Contributions of pressure $C_{L,p}$ and viscous force $C_{L,f}$ to the total lift coefficient C_L for $\alpha^* = 0.4$: (a) bubble (open symbols); (b) solid particle (closed symbols); (○, ●) C_L; (□, ■) $C_{L,p}$; (△, ▲) $C_{L,f}$.

lines indicate high and low values of the pressure lift contribution, and positive and negative values of the viscous lift contribution, respectively. The thick line in Fig. 9(c) shows the zero value of the viscous lift. Kurose and Komori (1999) explained the variations of $C_{L,p}$ and $C_{L,f}$ with Re_p for a solid particle as follows. Although the strong downward pressure lift appears on the front side of the solid particle (arrow A) for $Re_p = 1$ (see Fig. 9(b)), the moderately strong upward pressure lift is widely distributed over the bottom of the solid particle (this is confirmed by the contour lines distributed at the rear part). Further, the strong upward viscous lift appears widely on the lower part of the rear side (arrow C) compared with the strong downward one on the upper part. Therefore, both the integrated pressure lift and viscous lift over the whole surface, $C_{L,p}$ and $C_{L,f}$, show positive values. For high particle Reynolds number of $Re_p = 200$, the flow separations appear behind the solid particle (see Fig. 9(c)). The positions of the flow separations are indicated by arrows S in Fig. 9(c). The flow separation on the higher fluid-velocity side is located slightly upward compared to that on the lower fluid-velocity side. In addition to the strong downward pressure lift appearing on the front side of the solid particle (arrow A), strong pressure lifts caused

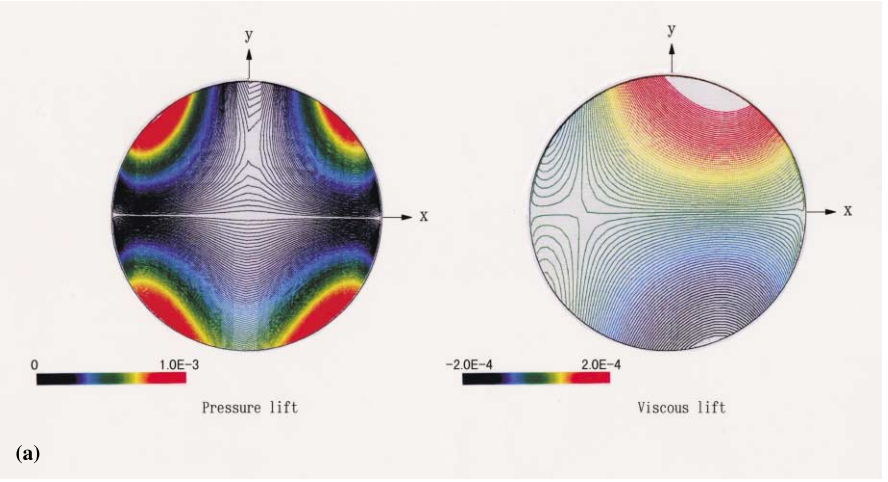
y
x
0
1.0E-3
Pressure lift
y
x
-2.0E-4
2.0E-4
Viscous lift

(a)

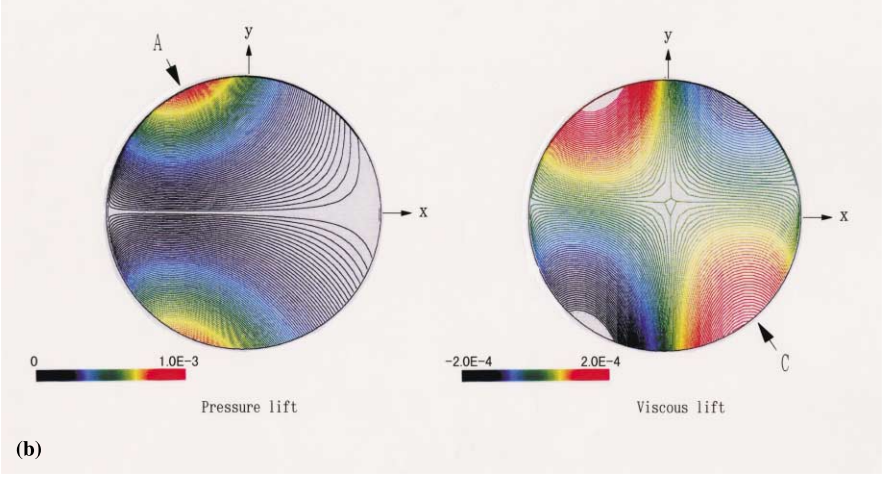
A
y
x
0
1.0E-3
Pressure lift
y
x
C
-2.0E-4
2.0E-4
Viscous lift

(b)

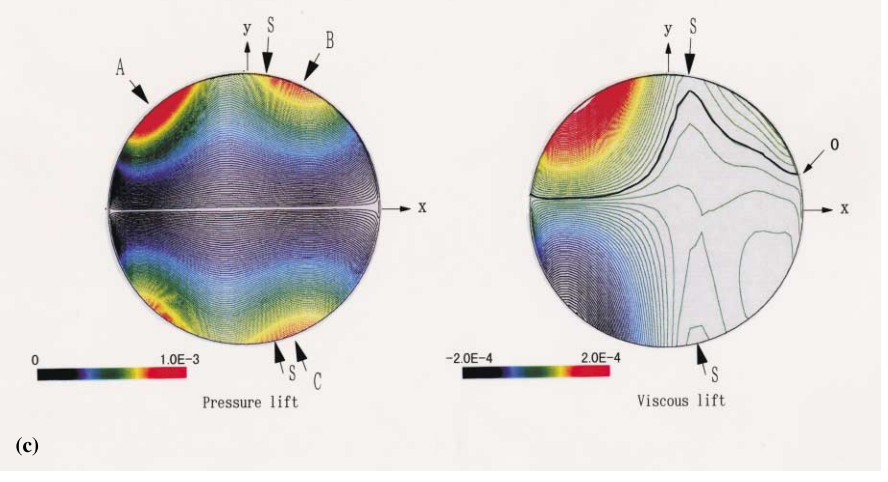
A
y
S
B
x
0
1.0E-3
S
C
Pressure lift
y
S
0
x
-2.0E-4
2.0E-4
S
Viscous lift

(c)

Fig. 9. Surface contours of the component for the pressure and viscous force in the y direction per unit area on a bubble and a solid particle in a linear shear flow for $\alpha^* = 0.2$: (a) bubble at $Re_p = 200$; (b) solid particle at $Re_p = 1$; (c) solid particle at $Re_p = 200$. The red and blue lines indicate high and low values of the pressure lift contribution, and positive and negative values of the viscous lift contribution, respectively. The thick line in (c) shows the zero value of the viscous lift.

by the flow separations also act on both the upper and lower parts of the rear side of the solid particle (arrows B and C). However, since the values of the pressure lift on the upper and lower parts of the rear side (arrows B and C) are roughly comparable, the strong downward pressure lift on the front side of the solid particle (arrow A) becomes dominant and therefore $C_{L,p}$ becomes negative. The downward viscous lift is widely distributed on the surface of the solid particle, and $C_{L,f}$ also shows negative values.

On the other hand, for a bubble at $Re_p = 200$, flow separations almost disappear, and the distribution of the pressure lift is symmetrical with regard to the y-axis (Fig. 9(a)). In contrast to the solid particle at $Re_p = 200$, for the bubble the upward and downward pressure lifts on the front side are almost comparable, and the upward pressure lift is widely exerted on the lower part. Also, the upward viscous lift on the upper part is slightly stronger than the downward viscous lift on the lower part. As a result, both $C_{L,p}$ and $C_{L,f}$ show positive values even for high particle Reynolds numbers.

4. Conclusions

A three-dimensional numerical simulation was done for a linear shear flow around a spherical bubble with high particle Reynolds numbers of $0.5 \leqslant Re_p \leqslant 200$, and the effects of fluid shear on drag and lift were investigated by comparing with the results of a solid particle.

The main results from this study can be summarized as follows:

(1) The fluid shear rate increases the drag on a spherical bubble, and the effect of the fluid shear is enhanced with increasing Re_p. The behavior of the drag is similar to that for a solid particle.

(2) The lift on a spherical bubble always acts to the higher fluid-velocity side, and the trend is quite different from that for a solid particle. The difference can well be explained by considering the pressure and viscous contributions to the lift.

Acknowledgements

This work was supported by the Japan Ministry of Education, Science and Culture through Grants-in-Aid (No. 11450077). The computations were conducted by the supercomputer of the Center for the Global Environmental Research, National Institute for Environmental Studies, Environment Agency of Japan.

References

Auton, T.R., 1987. The lift force on a spherical body in a rotational flow. J. Fluid Mech. 183, 199–218.
Clift, R., Grace, J.R., Weber, M.E., 1987. Bubble, Drops and Particles. Academic Press, New York.

Dandy, D.S., Dwyer, H.A., 1990. A sphere in shear flow at finite Reynolds number: effect of shear on particle lift, drag, and heat transfer. J. Fluid Mech. 216, 381–410.

Hanazaki, H., 1988. A numerical study of three-dimensional stratified flow past a sphere. J. Fluid Mech. 192, 393–419.

Kawamura, T., Kuwahara, K., 1984. Computation of high Reynolds number flow around a circular cylinder with surface roughness. AIAA paper 84-0340.

Komori, S., Kurose, R., 1996. The effects of shear and spin on particle lift and drag in shear flow at high Reynolds numbers. In: Gavrilakis, S., Machiels, L., Monkewitz, P. (Eds.), Advances in Turbulence, 4. Kluwer Academic Publishers, Dordrecht, pp. 551–554.

Kurose, R., Komori, S., 1999. Drag and lift forces on a rotating sphere in a linear shear flow. J. Fluid Mech. 384, 183–206.

Ligendre, D., Magnaudet, J., 1998. The lift force on a spherical bubble in a viscous linear shear flow. J. Fluid Mech. 368, 81–126.

Magnaudet, J., Rivero, M., Fabre, J., 1995. Accelerated flows past a rigid sphere or spherical bubble. Part I. Steady straining flow. J. Fluid Mech. 284, 97–135.

McLaughlin, J.B., 1991. Inertial migration of a small sphere in linear shear flows. J. Fluid Mech. 224, 261–274.

Mei, R., 1992. An approximate expression for the shear lift force on a spherical particle at finite Reynolds number. Int. J. Multiphase Flow 18, 145–147.

Mei, R., Klausner, J.F., 1994. Shear lift force on spherical bubbles. Int. J. Heat Fluid Flow 15, 62–65.

Moore, D.W., 1963. The boundary layer on a spherical gas bubble. J. Fluid Mech. 16, 161–176.

Saffman, P.G., 1965. The lift on a small sphere in a slow shear flow. J. Fluid Mech. 22, 385–400 (and Corrigendum, 31, 1968, 624).

Thames, F.C., Thompson, J.F., Mastin, C.W., Walker, R.L., 1977. Numerical solutions for viscous and potential flow about arbitrary two-dimensional bodies using body-fitted coordinate systems. J. Comput. Phys. 24, 245–273.